ARTICLES
https://doi.org/10.1038/s41592-018-0081-4
nature methods

Induction of myelinating oligodendrocytes in human cortical spheroids

Mayur Madhavan[1,5], Zachary S. Nevin[1,5], H. Elizabeth Shick[1], Eric Garrison[2], Cheryl Clarkson-Paredes[3], Molly Karl[2], Benjamin L. L. Clayton[1], Daniel C. Factor[1], Kevin C. Allan[1], Lilianne Barbar[1], Tanya Jain[4], Panagiotis Douvaras[4], Valentina Fossati[4], Robert H. Miller[2] and Paul J. Tesar[1*]

Cerebral organoids provide an accessible system for investigations of cellular composition, interactions, and organization but have lacked oligodendrocytes, the myelinating glia of the central nervous system. Here we reproducibly generated oligodendrocytes and myelin in 'oligocortical spheroids' derived from human pluripotent stem cells. Molecular features consistent with those of maturing oligodendrocytes and early myelin appeared by week 20 in culture, with further maturation and myelin compaction evident by week 30. Promyelinating drugs enhanced the rate and extent of oligodendrocyte generation and myelination, and spheroids generated from human subjects with a genetic myelin disorder recapitulated human disease phenotypes. Oligocortical spheroids provide a versatile platform for studies of myelination of the developing central nervous system and offer new opportunities for disease modeling and therapeutic development.

Advances in the generation of 3D tissues in vitro are improving the ability to study human neurodevelopment and disease[1–14]. Human pluripotent stem cell (hPSC)-derived 3D cultures—called organoids or spheroids—recapitulate complex developmental processes, cell–cell interactions, microenvironments, tissue architectures, and extended temporal dynamics that are inaccessible in traditional in vitro cultures[15,16]. Several groups have developed protocols to model the coordinated rounds of cell proliferation, migration, organization, and maturation required to pattern the human cerebral cortex[1,3,17]. These pluripotent-stem-cell-derived 'cortical spheroids' have been shown to generate various cortical cell types—including neural progenitors, mature neuron subtypes, and astrocytes—which self-organize into distinct cortical layers and establish functional neural networks[1–4,7–12,17,18]. However, although single-cell analyses of cortical spheroids have identified transcriptional profiles that suggest the presence of oligodendrocyte progenitor cells (OPCs)[7,10], and rare oligodendrocytes have been identified in isolation[19], so far no protocol has yielded reproducible generation and maturation of oligodendrocytes, the myelinating glia of the central nervous system (CNS) and one of three major cell types of neural origin.

Results

Generation of oligocortical spheroids. We generated OPCs and myelinating oligodendrocytes in hPSC-derived cortical spheroids by means of timed exposure to defined oligodendrocyte lineage growth factors and hormones. To start, we generated and patterned 'neurocortical spheroids', using an optimized version of a 50-d protocol[3]. After initial neurocortical patterning, we generated oligocortical spheroids by treating the neurocortical spheroids with platelet-derived growth factor AA (PDGF-AA) and insulin-like growth factor 1 (IGF-1) to drive the expansion of native OPC populations (days 50–60, corresponding to 'week 9'), followed by thyroid hormone (T3) to induce oligodendrocyte differentiation and, ultimately, myelination (days 60–70, or 'week 10') (Fig. 1a). PDGF-AA and IGF-1 are requisite developmental mitogens that promote the proliferation and survival of OPCs[20,21], and T3 has been shown to regulate and induce the generation of oligodendrocytes from OPCs in vivo[22]. Treatment time periods were empirically determined but mirror the initial specification of OPCs and oligodendrocytes in the human fetal brain at 10 and 14 weeks after conception, respectively[23,24].

We used human embryonic stem cell line H7 (female) for the initial development of the protocol. Then, to assess interline variability and demonstrate the robustness of our protocol, we reproduced key experiments with two additional independent hPSC lines: embryonic stem cell line H9 (female) and in-house-derived induced pluripotent stem cell (iPSC) line CWRU191 (male).

Induction of OPCs and oligodendrocytes. By the end of neurocortical patterning, at week 8, neurocortical spheroids contained few cells in the oligodendrocyte lineage, as evidenced by minimal immunostaining of OLIG2 and SOX10, two canonical OPC transcription factors (Supplementary Fig. 1b,c). However, subsequent treatment of patterned spheroids with PDGF-AA and IGF-1 for 10 d resulted in a substantial increase in the number of OPCs within the oligocortical spheroids compared with that in age-matched untreated neurocortical spheroids (Supplementary Fig. 1c–e).

By week 14, neurocortical spheroids had generated robust populations of neurons and astrocytes, but no oligodendrocytes (Fig. 1b), whereas oligocortical spheroids (treated with PDGF-AA and IGF-1 from days 50–60 and T3 from days 60–70) reproducibly generated robust populations of oligodendrocytes across all three hPSC lines, as demonstrated by immunofluorescence imaging for proteolipid protein 1 (PLP1), the most abundant oligodendrocyte membrane protein, and MYRF[25], a transcription factor specifically

[1]Department of Genetics and Genome Sciences, Case Western Reserve University School of Medicine, Cleveland, OH, USA. [2]Department of Anatomy and Regenerative Biology, George Washington University School of Medicine and Health Sciences, Washington, DC, USA. [3]Nanofabrication and Imaging Center, George Washington University School of Medicine and Health Sciences, Washington, DC, USA. [4]The New York Stem Cell Foundation Research Institute, New York, NY, USA. [5]These authors contributed equally: Mayur Madhavan, Zachary S. Nevin. *e-mail: paul.tesar@case.edu

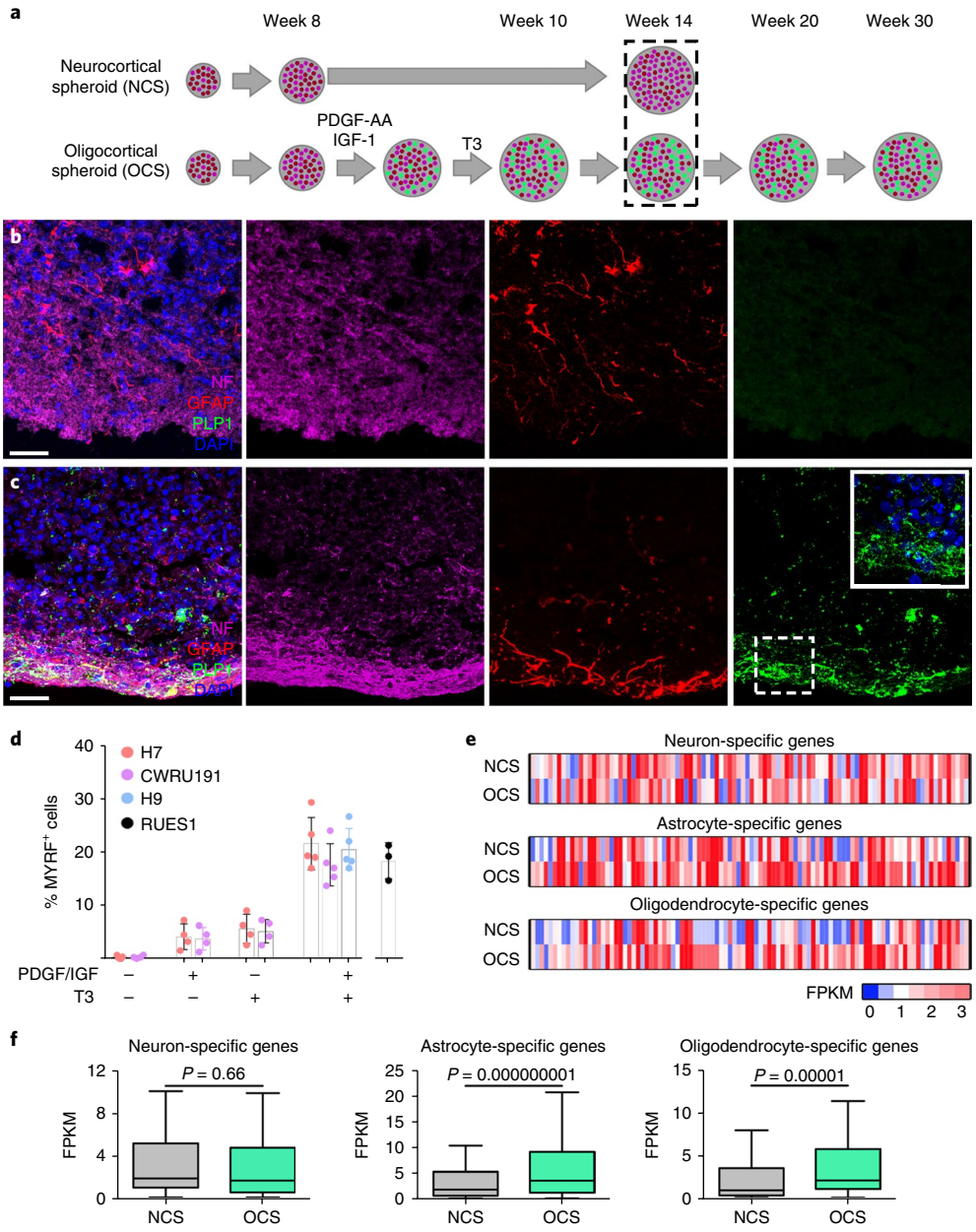

Fig. 1 | Generation of oligodendrocytes in human cortical spheroids. a, Schematic of spheroid generation. Protocols used to generate neurocortical spheroids and oligocortical spheroids were the same until week 8, after which time neurocortical spheroids were grown in basal media and oligocortical spheroids were treated with PDGF-AA and IGF-1 from days 50–60 and T3 from days 60–70. Differentiation of oligodendrocytes was assessed at week 14. Magenta, neurons; red, astrocytes; green, OPCs/oligodendrocytes. **b**,**c**, Representative fluorescence images of week 14 H7-cell-derived spheroids generated with the (**b**) neurocortical protocol or (**c**) oligocortical protocol. For each, similar results were obtained from 3 independent batches of spheroids generated from 4 separate lines. Scale bars, 50 µm; inset in **c** magnified 2.5× relative to the primary image. **b**, Neurocortical-protocol spheroids generated neurons (neurofilament (NF)) and astrocytes (GFAP), but no oligodendrocytes (PLP1). **c**, Oligocortical-protocol spheroids generated neurons (neurofilament), astrocytes (GFAP), and oligodendrocytes (PLP1). Inset, oligodendrocyte morphology in the outlined region, shown at higher magnification. **d**, Quantification of MYRF, a nuclear marker of the oligodendrocyte lineage, in week 14 spheroids generated with the neurocortical or oligocortical protocol and treated with various combinations of PDGF-AA, IGF-1, and T3. MYRF-positive cells were counted from four planes from four or five individual spheroids ($n=4$, PDGF-AA–IGF-1 or T3 treatments; $n=5$, NCS and OCS) for each treatment condition from lines H7, H9, and CWRU191. Data are shown as the average ± s.d. $n=3$ spheroids from the same batch were used for the externally validated cell line RUES1. **e**, Neuron, astrocyte, and oligodendrocyte gene expression in neurocortical and oligocortical spheroids. The heat maps represent the 100 top cell-specific transcripts for each cell type. Oligodendrocyte- and astrocyte-specific genes were upregulated in oligocortical compared with neurocortical spheroids. **f**, Neuron-, astrocyte-, and oligodendrocyte-specific gene expression from data in **e**. Box plots indicate the mean (center line) first and third quartiles (box edges), and maximum and minimum values (whiskers). **e**,**f**, RNA-seq data from 5 spheroids for each condition. Paired nonparametric Wilcoxon matched-pairs signed-rank test was used to determine significance. FPKM, fragments per kilobase of transcript per million mapped reads.

expressed in oligodendrocytes in the CNS (Fig. 1c, Supplementary Fig. 2a–c). Oligocortical spheroids exhibited low interline and interspheroid variability in the production of MYRF-positive oligodendrocytes, which constituted 21.59% ± 4.9%, 20.53% ± 3.9%, and 18.4% ± 2.2% of total cells (mean ± s.d.; a quantification schematic is presented in Supplementary Fig. 2c) in oligocortical spheroids derived from H7, H9, and CWRU191 cells, respectively, with $n=5$ spheroids per line (Fig. 1d). Additionally, robust induction

of the oligodendrocyte lineage was dependent on sequential treatment with both PDGF-AA and IGF-1 and then T3, as few MYRF-positive oligodendrocytes resulted from application of either treatment individually (Fig. 1d). Thus, while neurocortical patterning establishes the structural and cellular framework for oligodendrogenesis, PDGF-AA, IGF-1, and T3 are necessary for reproducible induction of OPCs and oligodendrocytes.

For further validation of the reproducibility of our approach, the protocol was replicated in an independent laboratory with an independent cell line, human embryonic stem cell line RUES1 (male)[26], and with separate personnel and reagents. MYRF-positive cells constituted 18.36% ± 3.37% of cells in the resulting RUES-derived oligocortical spheroids (Fig. 1d, Supplementary Fig. 2a,b).

Lastly, we used RNA sequencing of bulk spheroids to assess how PDGF-AA–IGF-1 and T3 treatments affected the global transcription of neuron, astrocyte, and oligodendrocyte genes in oligocortical spheroids compared with expression in age-matched neurocortical spheroids. Analysis of week 14 spheroids for the expression of the 100 most specific mRNA transcripts for each cell type (defined on the basis of mouse transcriptional data from https://brainrnaseq.org[27]) showed no significant changes in neuronal gene sets but significant upregulation of glial gene sets, in particular those of the oligodendrocyte lineage (Fig. 1e,f). These data show that this method for the generation of oligocortical spheroids activates a global oligodendrocyte transcriptional program but does not overtly alter the expression programs of other cell types in the spheroids, including neurons.

Oligodendrocyte maturation and myelination. After initial oligocortical patterning, spheroids can be maintained in basal media for weeks to months. We analyzed neuronal diversity and oligodendrocyte maturation at weeks 20 and 30 (Fig. 2a). Week 20 spheroids appeared to be relatively immature. In addition to MYRF-positive oligodendrocytes, they contained a large population of early-born deep-layer neurons marked by CTIP2 and a separate, smaller population of late-born superficial-layer neurons marked by SATB2, with MYRF-positive oligodendrocytes distributed throughout (Fig. 2b, Supplementary Fig. 3a). However, the neuron populations demonstrated substantial overlap, consistent with ongoing migration of younger SATB2 cells through the deep layers.

As oligodendrocytes mature, they extend cellular processes that track and myelinate adjacent axons. Although PLP1 expression was robust at as early as 14 weeks in culture, PLP1 immunofluorescence did not resolve into distinct processes until week 20 (Fig. 2c, Supplementary Fig. 3a). Furthermore, a subset of these processes began to express myelin basic protein (MBP; Fig. 2d), a marker of early myelin formation, suggesting that oligodendrocyte processes were associating with neuronal axons[28]. Electron microscopy (EM) revealed concentric, but often unorganized, wrapping of human axons with multiple layers of uncompacted myelin (Fig. 2e–g, Supplementary Fig. 3b) at week 20. Although the unorganized nature of this early oligocortical spheroid myelin can be attributed in part to the in vitro culture environment, it does show a striking resemblance to the earliest stages of in vivo fetal myelinogenesis in both humans and chicks[29,30]. Despite T3 treatment and extensive oligodendrocyte maturation, week 20 oligocortical spheroids also maintained a pool of SOX10-positive, MYRF-negative OPCs (Supplementary Fig. 3c).

At week 30, spheroids contained CTIP2- and SATB2-expressing neuron populations organized into distinct cortical layers, with a large SATB2-positive population and a smaller CTIP2-positive layer (Fig. 2h). MYRF-positive oligodendrocytes were present both throughout these layers and as a distinct layer adjacent to CTIP2-positive cells (Fig. 2h). Additionally, oligodendrocyte processes had further resolved into distinct PLP1-positive tracts that colocalized with neurofilament-expressing neuronal axons (Fig. 2i,j). EM at week 30 identified neuronal axons encircled by compact myelin (Fig. 2k), and serial block-face imaging with 3D reconstruction revealed longitudinal wraps of myelin ensheathing the axon (Fig. 2l). However, as of week 30 we could not identify definitive evidence of further structural organization, such as nodes of Ranvier, probably due in part to the continued immaturity and minimal coherent electrical activity of spheroid neurons (a noted issue with all current spheroid and organoid technologies).

Collectively, these results demonstrate that early myelination of human neurons by human oligodendrocytes can be generated in the context of oligocortical spheroids in as little as 20 weeks, with myelin maturation, refinement, and compaction by 30 weeks. This in vitro timing is similar to the timeline for the emergence of myelin in the latter part of the third trimester of human fetal development in utero[24], as well as the timing of human OPC maturation and myelination after transplantation to the rodent CNS[31,32], which suggests the potential presence of a cell-intrinsic developmental clock for human oligodendrocyte maturation, as proposed in rodents[33–35].

Relevance to in vivo cortical development. We next evaluated the developmental and cellular organization within our oligocortical spheroids to demonstrate relevance to in vivo human cortical development. By week 8, spheroids contained robust populations of dividing nestin-positive and SOX2-positive neural progenitors, organized into SOX2-positive ventricular-like and TBR2-positive outer subventricular-like zones (Fig. 3a,b). The arrangement of the SOX2-positive germinal centers was reminiscent of the ventricular zone in the cortex, although not all SOX2 populations surrounded a ventricle-like void, and many were localized to the outer surface of the spheroid. At week 9, we labeled proliferating SOX2-positive cells of these germinal centers with the thymidine analog 5-bromo-2′-deoxyuridine (BrdU) (Fig. 3c, Supplementary Fig. 4a) and tracked their developmental trajectories. By week 14, BrdU-labeled cells had migrated away from the germinal center, forming a population distinct from the SOX2-positive germinal zones (Fig. 3d,e, Supplementary Fig. 4a). At this time point, only oligocortical spheroids contained MYRF-positive OPCs, some of which were positive for both MYRF and BrdU (Fig. 3e, Supplementary Fig. 4a). MYRF colocalization with BrdU is strong evidence that these cells originated from BrdU-labeled SOX2-positive progenitors found in progenitor zones of the oligocortical spheroids.

The migration of BrdU-pulsed progenitors away from germinal centers suggests that oligocortical spheroids contain a continuum of proliferative and differentiating oligodendrocytes. To assess the global diversity of cellular composition and the spectrum of glial maturation, we carried out single-cell RNA-seq on oligocortical spheroids at week 12—an early time point just after PDGF-AA–IGF-1 and T3 treatment when all populations should be represented. Cell clustering broadly distinguished between glial and neuronal populations. The glial cluster contained early progenitors (marked by vimentin, SOX2, and nestin), OPCs (marked by SOX6), and maturing oligodendrocytes (marked by PLP1 and oligodendrocyte myelin glycoprotein) with expression of proliferative markers throughout the cluster and maturation markers defining progressively more distinct subpopulations (Supplementary Fig. 5a). This single-cell analysis demonstrates that distinct populations of oligodendrocytes at multiple stages of development coexist in oligocortical spheroids, similar to single-cell transcriptome data from human fetal cortex[36] (Supplementary Fig. 5a). This suggests that oligocortical spheroids might provide an avenue for interrogation of these largely inaccessible stages of human glial development.

Tests of promyelination drugs in spheroids. The ability to generate human oligodendrocytes that can myelinate human axons in an in vitro system provides new opportunities to explore human myelin development, disease, and therapeutics. We first tested

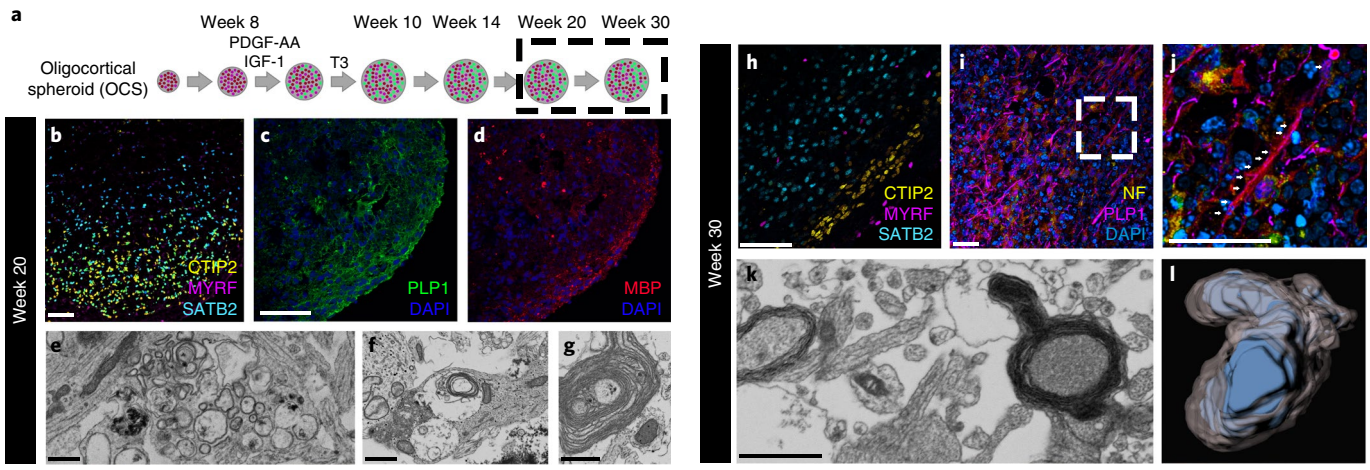

Fig. 2 | Maturation of oligodendrocytes in oligocortical spheroids. a, Schematic of oligocortical spheroid generation. Color-coding defined as in Fig. 1a. **b**–**d**, Representative fluorescence images of week 20 H7-cell-derived oligocortical spheroids. Similar results were obtained from 2 independent batches of spheroids. Scale bars, 50 µm (scale bar in **c** applies to **d**). **b**, Robust generation of oligodendrocyte-lineage (MYRF), CTIP2-positive early-born neurons, and SATB2-positive late-born neurons. **c**, Linear-process formation in maturing oligodendrocytes (PLP1). **d**, Immunostaining for MBP, a marker of mature myelin, showing punctate MBP expression indicative of an early stage of maturation. **e**–**g**, Representative EM images of week 20 H7-cell-derived oligocortical spheroids. EM results were obtained from a single batch of 3 spheroids. Scale bars, 1 µm. **e**, A cluster of neurons undergoing myelination by oligodendrocytes. **f**, An axon encircled by multiple layers of loosely compacted myelin. **g**, More extensive wrapping of loosely compacted myelin around an axon. **h**–**j**, Representative fluorescence images of week 30 H9-cell-derived oligocortical spheroids. Similar results were obtained from 4 spheroids from a single batch of oligocortical spheroids. Scale bars, 50 µm. **h**, Cortical lamination and separation of CTIP2-positive deep layers from SATB2-positive superficial layers. MYRF-positive oligodendrocytes are interspersed within the cortical layers. **i**, Oligodendrocyte processes (PLP1) track neuron axons (neurofilament (NF)). **j**, Higher-magnification image of the outlined region in **i**. Arrows indicate neuron axons. **k**, Electron micrograph of week 30 H9-cell-derived oligocortical spheroids showing compact myelin around axons. EM results were obtained from 3 spheroids from a single batch of spheroids Scale bar, 1 µm. **l**, 3D reconstruction from block-face EM sections taken along the length of an axon.

whether our human oligocortical spheroids recapitulate known effects of previously identified promyelination drugs. Our group and others have shown two drugs approved by the US Food and Drug Administration, clemastine and ketoconazole, to be potent stimulators of rodent oligodendrocyte generation and myelination in vitro and in vivo[37,38]. Moreover, clemastine was recently reported to enhance remyelination in a phase 2 repurposing clinical trial in human subjects with multiple sclerosis[39,40]. To assess the effect of these promyelination drugs on human oligodendrocyte generation, we treated oligocortical spheroids with PDGF-AA and IGF-1 from days 50–60, then with DMSO, T3, clemastine, or ketoconazole from days 60–70, and finally with basal medium for 4 weeks. Quantification of MYRF-positive oligodendrocytes at week 14 revealed that clemastine (18.7% ± 2.94%) and ketoconazole (27.61% ± 5.941%) each enhanced the production of oligodendrocytes to a similar extent as T3 (21.59% ± 4.9%) compared with production in vehicle (DMSO)-treated controls (6.345% ± 1.46%) (Fig. 4a–e). Remarkably, when examined by EM, ketoconazole-treated spheroids also exhibited myelination by week 14 of culture, 2 months earlier than T3-treated spheroids (Fig. 4f,g). These results demonstrate that clemastine and ketoconazole enhance and accelerate human oligodendrogenesis and maturation, and validate that oligocortical spheroids provide a physiological and species-relevant preclinical model for the evaluation of candidate myelin therapeutics prior to human clinical trials.

Spheroids recapitulate the pathology of a myelin disorder. Oligocortical spheroids provide an unprecedented tissue-like, minimally manipulated system in which to study hitherto inaccessible stages of human myelin formation and the pathologic processes that lead to myelin disease. We investigated the monogenic leukodystrophy Pelizaeus–Merzbacher disease (PMD; MIM number 312080) to test whether our system can recapitulate known cellular pathology and dysfunction. PMD is a rare X-linked disease associated with defects in myelin production[41]. Hundreds of mutations in the causal gene *PLP1* have been identified in patients, who present with a spectrum of severity ranging from mild motor delay and spasticity to severe hypotonia with early childhood mortality.

We previously used 2D culture[42] to generate PMD oligodendrocytes derived from iPSCs from a panel of affected male subjects[28], and demonstrated both distinct and convergent cellular phenotypes in individuals with various mutations. Here we generated oligocortical spheroids from three iPSC lines with different PMD-related mutations: deletion of the entire *PLP1* locus, duplication of the entire *PLP1* locus, and a point mutation in *PLP1* (c.254T>G). Phenotypically, the respective subjects were mildly (deletion), moderately (duplication), and severely (point mutation) affected. To control for both gender and cell type of origin, we simultaneously generated spheroids from a healthy control male iPSC line derived in-house, CWRU198, that expressed MYRF (18.4% ± 2.20%) and PLP1 (Fig. 5a,b) to similar extents as the previously described control lines H7, H9, and CWRU191.

In oligocortical spheroids, the abundance of MYRF-positive oligodendrocytes trended with disease severity, whereas the extent of PLP1 expression correlated with genetic status (Fig. 5c–h). The *PLP1*-deletion line produced abundant MYRF-positive oligodendrocytes (15.14% ± 1.96%), despite the expected absence of PLP1 (Fig. 5c,d,m). Conversely, the duplication line produced abundant PLP1 signal (Fig. 5e), despite a significant decrease in the number of MYRF-positive oligodendrocytes (11.84% ± 2.27%) compared with that in CWRU198 cells (Fig. 5f,m). In previous 2D cultures[28], oligodendrocytes bearing the c.254T>G point mutation showed distinct perinuclear retention of PLP1 that resolved after chemical modulation of the endoplasmic reticulum (ER) stress pathway. Oligocortical spheroids recapitulated this phenotype, demonstrating frank perinuclear retention of PLP1 (Fig. 5g) and the most severe reduction in the number of MYRF-positive oligodendrocytes (9.69% ± 1.82%) (Fig. 5h,m). Subsequent treatment of point-mutation oligocortical

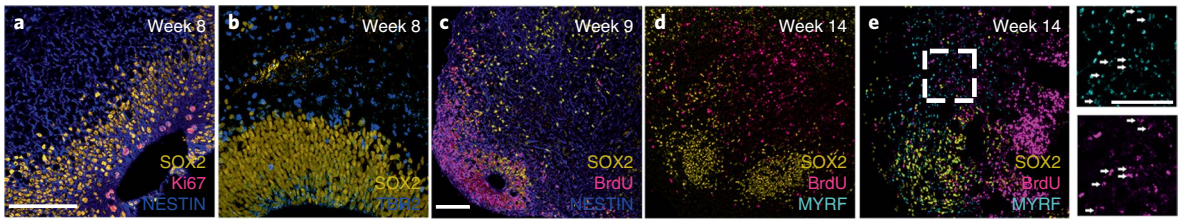

Fig. 3 | Cortical patterning and organization in oligocortical spheroids. a,**b**, Representative fluorescence images of week 8 H7-cell-derived spheroids. **a**, At the end of initial neurocortical patterning, spheroids generated distinct populations of neural progenitors (SOX2 and nestin) that organized into ventricular-like zones. These cells were also the only actively dividing cells, as indicated by Ki67 expression. **b**, A TBR2-positive outer subventricular-zone-like area appeared adjacent to the SOX2-positive ventricular-like area. **c**, Representative fluorescence image of H7-cell-derived spheroids generated with the oligocortical protocol up through PDGF-AA–IGF-1 treatment, then treated with two doses of BrdU during week 9 (days 58 and 60) to label dividing cells. BrdU-positive cells localized to SOX2-positive ventricular zones, thus identifying this as a primary germinal center. **d**,**e**, Representative fluorescence images of H7-cell-derived spheroids generated with either the neurocortical (**d**) or the oligocortical (**e**) protocol, treated with BrdU during week 9 (days 58 and 60), and then maintained through week 14. Only oligocortical spheroids generated oligodendrocytes (MYRF), many of which were also positive for BrdU (indicated by arrows in higher-magnification (2×) views of the outlined region in **e** (right)). Scale bars, 50 µm; scale bar in **a** applies to **b**, and scale bar in **c** applies to **d** and lower-magnification image in **e**.

spheroids with GSK2656157, an inhibitor of protein-kinase-R-like ER kinase[43], improved mobilization of PLP1 away from the ER and into oligodendrocyte processes (Fig. 5i) and significantly increased the percentage of MYRF-positive cells (15.04% ± 1.96%) (Fig. 5j,m). Lastly, CRISPR correction of the point mutation to the wild-type sequence (Supplementary Fig. 6a–c) in iPSCs prior to oligocortical spheroid generation not only restored PLP1 mobilization into oligodendrocyte processes (Fig. 5k), but also increased the percentage of MYRF-positive oligodendrocytes (17.25% ± 3.22%) back to the levels in healthy controls (Fig. 5l,m) and enabled myelin generation by 20 weeks in culture (Fig. 5n).

The mechanistic relationships between PMD genotypes and phenotypes have not been fully characterized. Current data suggest that the accumulation of excess (e.g., duplicated) PLP1 or aberrant/misfolded (e.g., missense mutant) PLP1 leads to ER stress, cell death, and severe patient phenotypes, whereas PLP1 deletion is better tolerated[44], and the dichotomy between cell abundance and PLP1 expression in our oligocortical spheroids is in agreement with this hypothesis. hPSC-derived brain organoids and cortical spheroids have been used to investigate mutation-specific pathologic processes involved in neuronal disorders[2,45–47]. Having validated our system, we can extend these efforts to a wide variety of myelin diseases and begin to explore patient-specific pathogenesis over the course of oligodendrocyte birth, maturation, myelination, and death.

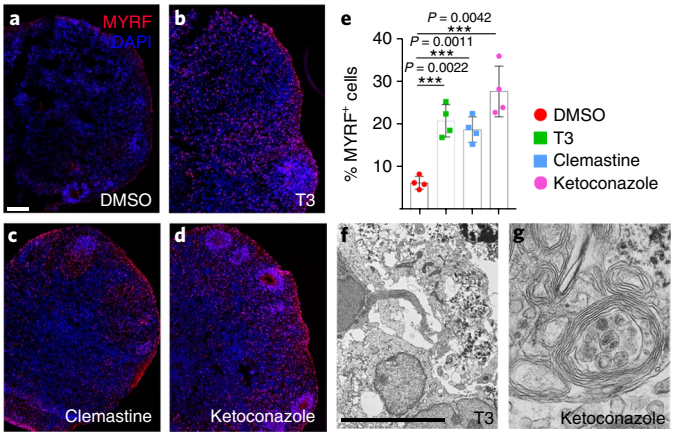

Fig. 4 | Promyelination drugs promote the generation of oligodendrocytes in oligocortical spheroids. a–**d**, Representative fluorescence images of week 14 H7-cell-derived spheroids treated with PDGF-AA and IGF-1 (from days 50–60) plus (**a**) DMSO, (**b**) T3, (**c**) clemastine, or (**d**) ketoconazole (from days 60–70). Whereas DMSO treatment produced few MYRF-positive cells, treatment with T3, clemastine, or ketoconazole produced robust MYRF signal. Four spheroids from the same batch were used for analysis. Scale bar, 50 µm (scale bar in **a** applies to **b**–**d**). **e**, Quantification of MYRF from **a**–**d**. MYRF-positive cells were counted in $n = 4$ individual spheroids per cell line (colored symbols); data are shown as the average ± s.d. Significance determined by two-tailed unpaired *t*-test with Welch's correction. **f**,**g**, Representative EM images of week 14 H7-cell-derived spheroids. Scale bar, 500 nm (applies to both panels). **f**, Spheroids generated with the standard oligocortical protocol (T3), demonstrating an absence of myelin. **g**, Spheroids generated with ketoconazole in lieu of T3, demonstrating robust production of non-compact myelin encircling multiple neuronal axons.

Discussion

Human corticogenesis is a complex process that requires the coordinated generation, migration, and maturation of distinct cell populations. While many groups have generated oligodendrocytes through in vitro 2D cultures[31,42] and forced aggregation of differentiating neural cells[48], hPSC-derived cortical spheroids harness intrinsic differentiation programs to recapitulate regional organization and cortical layering present in the developing human brain. Here we demonstrated a method to induce oligodendrocyte progenitors and myelinating oligodendrocytes in cortical spheroids by exposing them to growth factors PDGF, IGF-1, and T3, while preserving the general organization and regional specification demonstrated in prior neuronal models. Further work is required to refine cortical architecture in these spheroids, but the induction of all major CNS lineages provides a new opportunity to observe and perturb human cortical development and disease.

In validating our system, we demonstrated applications in genetic disease modeling and preclinical drug screening. Oligocortical spheroids could be used to study many challenging concepts, from demyelination in leukodystrophies to possible remyelination strategies for people with multiple sclerosis. With further development, this system could also be used to explore basic questions of myelin development in different neuronal classes, myelin compaction, node and internode size modulation, and single-neuron and whole-spheroid electrophysiology. Regional populations of oligodendrocytes arise, migrate, and mature at distinct times during embryogenesis. In mammals, ventrally derived oligodendrocytes are among the first populations to arise, yet they are not required for proper myelination of the cortex and are mostly replaced by later

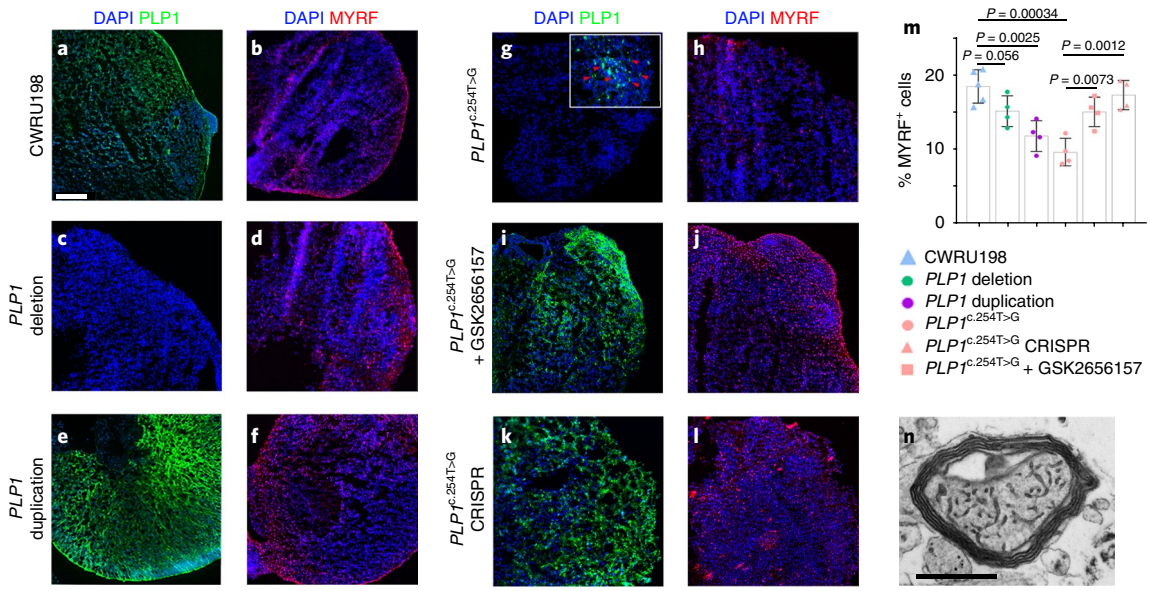

Fig. 5 | Oligocortical spheroids recapitulate a human myelin disease phenotype. a–l, Representative fluorescence images of week 14 oligocortical spheroids. Five (**a**,**b**) or four (**c**–**l**) spheroids from the same batch were used for analysis. Scale bar, 50 µm (applies to all panels). **a**,**b**, CWRU198 spheroids immunostained for (**a**) PLP1 or (**b**) MYRF show abundant oligodendrocytes and robust PLP1 expression. **c**,**d**, *PLP1*-deletion spheroids immunostained for (**c**) PLP1 or (**d**) MYRF show an expected lack of PLP1 despite abundant MYRF-positive oligodendrocytes. **e**,**f**, *PLP1*-duplication oligocortical spheroids immunostained for (**e**) PLP1 or (**f**) MYRF show robust PLP1 expression despite decreased abundance of MYRF-positive oligodendrocytes. **g**,**h**, *PLP1* c.254T>G spheroids immunostained for (**g**) PLP1 or (**h**) MYRF demonstrate perinuclear retention of PLP1 and decreased MYRF-positive oligodendrocyte abundance. **i**,**j**, *PLP1* c.254T>G oligocortical spheroids treated with GSK2656157 and immunostained for (**i**) PLP1 or (**j**) MYRF demonstrate mobilization of PLP1 into oligodendrocyte processes and rescue of MYRF-positive oligodendrocyte abundance. **k**,**l**, *PLP1* CRISPR-corrected c.254G>T oligocortical spheroids immunostained for (**k**) PLP1 or (**l**) MYRF demonstrate rescue of both PLP1 perinuclear retention and oligodendrocyte abundance. **m**, Percentage of MYRF-positive oligodendrocytes per organoid in **a**–**l**. MYRF-positive cells were counted from $n = 5$ individual spheroids of control line CWRU198 and $n = 4$ individual spheroids per cell line; data are shown as the average ± s.d. Significance determined by two-tailed unpaired *t*-test with Welch's correction. **n**, Representative EM image of week 30 *PLP1* CRISPR-corrected c.254G>T oligocortical spheroids, showing compact myelin encircling an axon. Three spheroids from a single batch were used for EM analysis. Scale bar, 1 µm.

cortex-derived oligodendrocytes[49]. Even compared with that of non-human primates, the timing and duration of human myelination is regionally distinct[50]. Human-cell-derived oligocortical spheroids provide an accessible system in which to explore these and other unique aspects of human myelin development.

Received: 11 May 2018; Accepted: 2 July 2018;
Published online: 25 July 2018

References

1. Kadoshima, T. et al. Self-organization of axial polarity, inside-out layer pattern, and species-specific progenitor dynamics in human ES cell-derived neocortex. *Proc. Natl. Acad. Sci. USA* **110**, 20284–20289 (2013).
2. Lancaster, M. A. et al. Cerebral organoids model human brain development and microcephaly. *Nature* **501**, 373–379 (2013).
3. Paşca, A. M. et al. Functional cortical neurons and astrocytes from human pluripotent stem cells in 3D culture. *Nat. Methods* **12**, 671–678 (2015).
4. Camp, J. G. et al. Human cerebral organoids recapitulate gene expression programs of fetal neocortex development. *Proc. Natl. Acad. Sci. USA* **112**, 15672–15677 (2015).
5. Jo, J. et al. Midbrain-like organoids from human pluripotent stem cells contain functional dopaminergic and neuromelanin-producing neurons. *Cell Stem Cell* **19**, 248–257 (2016).
6. Bagley, J. A., Reumann, D., Bian, S., Lévi-Strauss, J. & Knoblich, J. A. Fused cerebral organoids model interactions between brain regions. *Nat. Methods* **14**, 743–751 (2017).
7. Birey, F. et al. Assembly of functionally integrated human forebrain spheroids. *Nature* **545**, 54–59 (2017).
8. Lancaster, M. A. et al. Guided self-organization and cortical plate formation in human brain organoids. *Nat. Biotechnol.* **35**, 659–666 (2017).
9. Li, Y. et al. Induction of expansion and folding in human cerebral organoids. *Cell Stem Cell* **20**, 385–396 (2017).
10. Quadrato, G. et al. Cell diversity and network dynamics in photosensitive human brain organoids. *Nature* **545**, 48–53 (2017).
11. Renner, M. et al. Self-organized developmental patterning and differentiation in cerebral organoids. *EMBO J.* **36**, 1316–1329 (2017).
12. Sloan, S. A. et al. Human astrocyte maturation captured in 3D cerebral cortical spheroids derived from pluripotent stem cells. *Neuron* **95**, 779–790 (2017).
13. Xiang, Y. et al. Fusion of regionally specified hPSC-derived organoids models human brain development and interneuron migration. *Cell Stem Cell* **21**, 383–398 (2017).
14. Nakano, T. et al. Self-formation of optic cups and storable stratified neural retina from human ESCs. *Cell Stem Cell* **10**, 771–785 (2012).
15. Paşca, S. P. The rise of three-dimensional human brain cultures. *Nature* **553**, 437–445 (2018).
16. Arlotta, P. Organoids required! A new path to understanding human brain development and disease. *Nat. Methods* **15**, 27–29 (2018).
17. Lancaster, M. A. & Knoblich, J. A. Generation of cerebral organoids from human pluripotent stem cells. *Nat. Protoc.* **9**, 2329–2340 (2014).
18. Luo, C. et al. Cerebral organoids recapitulate epigenomic signatures of the human fetal brain. *Cell Rep.* **17**, 3369–3384 (2016).
19. Monzel, A. S. et al. Derivation of human midbrain-specific organoids from neuroepithelial stem cells. *Stem Cell Rep.* **8**, 1144–1154 (2017).
20. McMorris, F. A., Smith, T. M., DeSalvo, S. & Furlanetto, R. W. Insulin-like growth factor I/somatomedin C: a potent inducer of oligodendrocyte development. *Proc. Natl. Acad. Sci. USA* **83**, 822–826 (1986).
21. Noble, M., Murray, K., Stroobant, P., Waterfield, M. D. & Riddle, P. Platelet-derived growth factor promotes division and motility and inhibits premature differentiation of the oligodendrocyte/type-2 astrocyte progenitor cell. *Nature* **333**, 560–562 (1988).
22. Barres, B. A., Lazar, M. A. & Raff, M. C. A novel role for thyroid hormone, glucocorticoids and retinoic acid in timing oligodendrocyte development. *Development* **120**, 1097–1108 (1994).
23. Jakovcevski, I., Filipovic, R., Mo, Z., Rakic, S. & Zecevic, N. Oligodendrocyte development and the onset of myelination in the human fetal brain. *Front. Neuroanat.* **3**, 5 (2009).
24. Silbereis, J. C., Pochareddy, S., Zhu, Y., Li, M. & Sestan, N. The cellular and molecular landscapes of the developing human central nervous system. *Neuron* **89**, 248–268 (2016).

25. Bujalka, H. et al. MYRF is a membrane-associated transcription factor that autoproteolytically cleaves to directly activate myelin genes. *PLoS Biol.* **11**, e1001625 (2013).
26. James, D., Noggle, S. A., Swigut, T. & Brivanlou, A. H. Contribution of human embryonic stem cells to mouse blastocysts. *Dev. Biol.* **295**, 90–102 (2006).
27. Zhang, Y. et al. An RNA-sequencing transcriptome and splicing database of glia, neurons, and vascular cells of the cerebral cortex. *J. Neurosci.* **34**, 11929–11947 (2014).
28. Nevin, Z. S. et al. Modeling the mutational and phenotypic landscapes of Pelizaeus-Merzbacher disease with human iPSC-derived oligodendrocytes. *Am. J. Hum. Genet.* **100**, 617–634 (2017).
29. Weidenheim, K. M., Kress, Y., Epshteyn, I., Rashbaum, W. K. & Lyman, W. D. Early myelination in the human fetal lumbosacral spinal cord: characterization by light and electron microscopy. *J. Neuropathol. Exp. Neurol.* **51**, 142–149 (1992).
30. Szuchet, S., Nielsen, L. L., Domowicz, M. S., Austin, J. R. II & Arvanitis, D. L. CNS myelin sheath is stochastically built by homotypic fusion of myelin membranes within the bounds of an oligodendrocyte process. *J. Struct. Biol.* **190**, 56–72 (2015).
31. Wang, S. et al. Human iPSC-derived oligodendrocyte progenitor cells can myelinate and rescue a mouse model of congenital hypomyelination. *Cell Stem Cell* **12**, 252–264 (2013).
32. Windrem, M. S. et al. Human iPSC glial mouse chimeras reveal glial contributions to schizophrenia. *Cell Stem Cell* **21**, 195–208 (2017).
33. Gao, F. B., Durand, B. & Raff, M. Oligodendrocyte precursor cells count time but not cell divisions before differentiation. *Curr. Biol.* **7**, 152–155 (1997).
34. Raff, M. C., Lillien, L. E., Richardson, W. D., Burne, J. F. & Noble, M. D. Platelet-derived growth factor from astrocytes drives the clock that times oligodendrocyte development in culture. *Nature* **333**, 562–565 (1988).
35. Temple, S. & Raff, M. C. Clonal analysis of oligodendrocyte development in culture: evidence for a developmental clock that counts cell divisions. *Cell* **44**, 773–779 (1986).
36. Nowakowski, T. J. et al. Spatiotemporal gene expression trajectories reveal developmental hierarchies of the human cortex. *Science* **358**, 1318–1323 (2017).
37. Najm, F. J. et al. Drug-based modulation of endogenous stem cells promotes functional remyelination in vivo. *Nature* **522**, 216–220 (2015).
38. Mei, F. et al. Micropillar arrays as a high-throughput screening platform for therapeutics in multiple sclerosis. *Nat. Med.* **20**, 954–960 (2014).
39. Cohen, J. A. & Tesar, P. J. Clemastine fumarate for promotion of optic nerve remyelination. *Lancet* **390**, 2421–2422 (2017).
40. Green, A. J. et al. Clemastine fumarate as a remyelinating therapy for multiple sclerosis (ReBUILD): a randomised, controlled, double-blind, crossover trial. *Lancet* **390**, 2481–2489 (2017).
41. Hobson, G. M. & Garbern, J. Y. Pelizaeus-Merzbacher disease, Pelizaeus-Merzbacher-like disease 1, and related hypomyelinating disorders. *Semin. Neurol.* **32**, 62–67 (2012).
42. Douvaras, P. et al. Efficient generation of myelinating oligodendrocytes from primary progressive multiple sclerosis patients by induced pluripotent stem cells. *Stem Cell Rep.* **3**, 250–259 (2014).
43. Axten, J. M. et al. Discovery of GSK2656157: an optimized PERK inhibitor selected for preclinical development. *ACS Med. Chem. Lett.* **4**, 964–968 (2013).
44. Garbern, J. Y. Pelizaeus-Merzbacher disease: genetic and cellular pathogenesis. *Cell. Mol. Life Sci.* **64**, 50–65 (2007).
45. Bershteyn, M. et al. Human iPSC-derived cerebral organoids model cellular features of lissencephaly and reveal prolonged mitosis of outer radial glia. *Cell Stem Cell* **20**, 435–449 (2017).
46. Mariani, J. et al. FOXG1-dependent dysregulation of GABA/glutamate neuron differentiation in autism spectrum disorders. *Cell* **162**, 375–390 (2015).
47. Qian, X. et al. Brain-region-specific organoids using mini-bioreactors for modeling ZIKV exposure. *Cell* **165**, 1238–1254 (2016).
48. Pamies, D. et al. A human brain microphysiological system derived from induced pluripotent stem cells to study neurological diseases and toxicity. *ALTEX* **34**, 362–376 (2017).
49. Kessaris, N. et al. Competing waves of oligodendrocytes in the forebrain and postnatal elimination of an embryonic lineage. *Nat. Neurosci.* **9**, 173–179 (2006).
50. Miller, D. J. et al. Prolonged myelination in human neocortical evolution. *Proc. Natl Acad. Sci. USA* **109**, 16480–16485 (2012).

Acknowledgements

This research was supported by the NIH (R01NS093357 to P.J.T.; R01NS095280 to P.J.T. and R.H.M.; T32GM007250 and F30HD084167 to Z.S.N.), the Pelizaeus-Merzbacher Disease Foundation (P.J.T.), the New York Stem Cell Foundation (P.J.T.), the Connor B. Judge Foundation (P.J.T.), the New York Stem Cell Foundation Research Institute (V.F.), the National Stem Cell Foundation (T.J. and V.F.), and philanthropic support from the Peterson, Fakhouri, Long, Goodman, Geller, Galbut/Heil, and Weidenthal families. Additional support was provided by the CWRU SOM Light Microscopy Core Facility (S10-OD016164) and the Genomics core facility of the Case Comprehensive Cancer Center (P30CA043703). We are grateful to B. Nawash, C. Blake, M. Cartwright, M. Cameron, R. Lee, A. Miron, S. Edelheit, M. Hitomi, F. Pirozzi, and A. Wynshaw-Boris for technical assistance and discussion. Rat anti-PLP1 was a gift from W. Macklin (University of Colorado Anschutz Medical Campus, Aurora, CO, USA); rabbit anti-MYRF was provided by M. Wegner (Institut für Biochemie, Emil-Fischer-Zentrum, Universität Erlangen-Nürnberg, Erlangen, Germany).

Author contributions

M.M., Z.S.N., and P.J.T. conceived and initiated the project. M.M. and Z.S.N. developed the oligocortical spheroid protocol and generated spheroids for all experiments. M.M., H.E.S., B.L.L.C., K.C.A., and L.B. performed immunohistochemistry and quantification and generated associated figures. D.C.F. and B.L.L.C. analyzed RNA-seq data and generated associated figures. E.G., C.C.-P., M.K., and R.H.M. designed and performed electron microscopy experiments and analysis and generated associated figures. H.E.S. maintained hPSC lines. T.J., P.D., and V.F. independently replicated the oligocortical spheroid protocol. Z.S.N., M.M., and P.J.T. wrote the manuscript with input from all other authors.

Competing interests

P.J.T. and R.H.M. are consultants for Convelo Therapeutics, which has licensed patents from Case Western Reserve University. P.J.T., R.H.M., and Case Western Reserve University hold equity in Convelo Therapeutics. D.C.F. became an employee of Convelo Therapeutics subsequent to the completion of these studies. P.J.T. is a consultant and on the Scientific Advisory Board of Cell Line Genetics. P.J.T. is chair of the Scientific Advisory Board (volunteer position) for the Pelizaeus-Merzbacher Disease Foundation.

Additional information

Supplementary information is available for this paper at https://doi.org/10.1038/s41592-018-0081-4.

Reprints and permissions information is available at www.nature.com/reprints.

Correspondence and requests for materials should be addressed to P.J.T.

Methods

Pluripotent stem cell lines. Healthy (CWRU191 and CWRU198) and PMD iPSCs were generated prior to this study after receipt of informed consent and approval by the Case Western Reserve University and University Hospital Institutional Review Board[28,51]. Two human embryonic stem cell (hESC) lines from the approved NIH hESC Registry (H7, NIHhESC-10-0061; H9, NIHhESC-10-0062) were also used in these studies.

Oligocortical spheroid differentiation. Neurocortical spheroids were generated from hPSCs as previously described, with variations noted below[3].

For patterning of neurocortical spheroids, pluripotent stem cell colonies cultured on vitronectin (Gibco; A14700) were lifted with dispase (Gibco; 17105-041) at 37 °C for 10 min. Intact colonies were transferred to individual low-adherence V-bottom 96-well plates (S-Bio Prime; MS-9096VZ) in 200 µl of spheroid starter media with 10 µM ROCK inhibitor Y-27632 (Calbiochem; 688001), 10 µM dorsopmorphin (Sigma; P5499), and 10 µM SB-431542 (Sigma; S4317). Spheroid starter media was DMEM/F12 (Invitrogen; 11320-033) containing 20% KnockOut Serum (Invitrogen; 12587-010), non-essential amino acids (Invitrogen; 11140050), Glutamax (Invitrogen; 35050061), β-mercaptoethanol, and 100 U/ml penicillin–streptomycin. The same media without ROCK inhibitor was used for the next 5 d, after which the media was changed to Neurobasal-A-based spheroid media. Neurobasal-A spheroid media was Neurobasal-A medium (Invitrogen; 10888022) with B-27 serum substitute without vitamin A (Invitrogen; 12587), Glutamax (Invitrogen; 35050061), and 100 U/ml penicillin–streptomycin. From day 7 to day 25, 20 ng/ml FGF-2 (R&D Systems; 233-FB-25/CF) and 10 ng/ml EGF (R&D Systems; 236-EG-200) were added to the media. Spheroids were cultured in 96-well plates through day 25, with daily half-media changes. On day 25, spheroids were transferred to ultra-low-attachment six-well plates (Corning; CLS3471) at a density of 8–10 spheroids per well and cultured thus through the remainder of the protocol. Also from this point forward, 1% Geltrex (Invitrogen; A15696-01) was added to the Neurobasal-A spheroid media. Neural differentiation was induced between days 27 and 41 by supplementation of Neurobasal-A spheroid media with 20 ng/ml BDNF (R&D Systems; 248-BD) and 20 ng/ml NT-3 (R&D Systems; 267-N). Half-media changes were performed every other day between days 17 and 41.

To generate oligocortical spheroids, beginning on day 50, we added 10 ng/ml PDGF-AA (R&D Systems; 221-AA-050) and 10 ng/ml IGF-1 (R&D Systems; 291-G1-200) to the every-other-day media changes for 10 d. Next, on day 60, we added 40 ng/ml 3,3′,5-triiodothronine (T3; Sigma; ST2877) to the every-other-day media changes for 10 d. When used, small molecules were supplemented during this period. 4 µM ketoconazole and 2 µM clemastine were added in lieu of T3. GSK2656157 was added in addition to T3.

After day 70, spheroids were matured and maintained in Neurobasal-A spheroid media with every-other-day media changes until completion of the experiment.

Independent validation. One hESC line, RUES1, from the approved NIH hESC Registry (NIHhESC-09-0012) was used. RUES1 cells were cultured on Matrigel in mTeSR1 medium (Stemcell Technologies; 85850) and lifted with StemPro Accutase (Thermo Fisher; A1110501). Oligocortical spheroid differentiation was performed as described above, with the exception of the use of N2 supplement (Thermo Fisher; 17502048) and 25 mg/ml human insulin solution (Sigma; I9278) in place of KnockOut serum replacement for days 1–7 of the differentiation protocol.

Small molecules. 4 mM stock solution of ketoconazole (Sigma; K1003), 2 mM stock solution of clemastine fumarate (Sigma; SML0445), and 10 mM stock solution of GSK2656157 (EMD Millipore; 5046510001) were prepared, aliquoted, and stored at −20 °C. Small molecules were warmed to 37 °C for 20 min before being added to prewarmed medium. Frozen aliquots were thawed no more than twice before being discarded.

BrdU labeling. To label dividing cells in spheroids, we added BrdU to culture media at a final concentration of 3 µg/ml on days 58 and 60. Week 9 samples were collected 4 h after BrdU administration on day 60. For lineage-tracing experiments, BrdU-labeled spheroids were collected on week 14 and processed for immunohistochemistry.

PLP1 gene editing. CRISPR–Cas9 editing of a *PLP1* point mutation (c.254T>G) in iPSCs was performed by the Genome Engineering and iPSC Center at Washington University in St. Louis, using a guide RNA overlapping the mutation (sequence: CCAGCAGGCGGGCCCCATAAAGG) and a single-strand oligonucleotide with 25-nt homology arms surrounding the mutation. Upon receipt, we resequenced the mutation and correction locus and karyotyped both lines in-house to ensure that no gross genotypic aberrations were generated during the editing process (Cell Line Genetics).

Immunocytochemistry. Spheroids for immunohistochemistry were initially fixed with 4% ice-cold paraformaldehyde for 45 min, washed three times in PBS, and equilibrated with 30% sucrose overnight. The spheroids were embedded in OCT and sectioned at 10 µm.

Immunohistochemistry was performed as described previously[52]. Briefly, sections were washed in PBS three times and then blocked for 30 min in PBS containing 0.1% Triton X-100 and 0.25% normal donkey serum. The sections were then incubated at 4 °C overnight with primary antibodies in blocking solution. We used the following primary antibodies: rat anti-PLP1 (1:500; AA3; gift from Wendy Macklin), rabbit anti-MYRF (1:1,000; provided by Michael Wegner), goat anti-SOX10 (1:250; R&D Systems; AF 2864), rabbit anti-OLIG2 (1:250; Millipore; AB9610), mouse anti-pan-axonal neurofilament (1:1,000, Covance; SMI311), mouse anti-MBP (1:200; Covance; Smi99), mouse anti-pan-neuronal neurofilament (NF; 1:1,000; Covance; SMI312), rabbit anti-GFAP (1:1,000; Dako; Z0334), mouse anti-SATB2 (1:250; Abcam; ab51520), rat anti-CTIP2 (1:400; Abcam; ab18465), goat anti-SOX2 (1:250; R&D Systems; AF2018), rabbit anti-TBR2 (1:250; Abcam; ab23345), mouse anti-Ki67 (1:250; Millipore; MAB4190), mouse anti-nestin (1:1,000; Millipore; MAB5326), mouse anti-BrdU (1:1,000; Millipore; MAB3510), chicken anti-vimentin (1:1,000; Abcam; ab24525); and DAPI (1 µg/ml; Sigma; D8417). Sections were then washed in PBS and incubated in secondary antibodies for 2 h. All secondary antibodies were Life Technologies Alexa Fluor–conjugated secondary antibodies used at a dilution of 1:500. In the case of PLP1 immunohistochemistry, a 20-min wash in PBS containing 10% Triton X-100 was applied before the blocking step. In the case of MBP immunohistochemistry, we applied a 20-min post-fixation step using ice-cold acetone. After antigen retrieval we performed BrdU immunohistochemistry, which entailed placing slides in a sealed Coplin jar with boiling 100 mM sodium citrate buffer and allowing it to come to room temperature over the course of 1 h.

Spheroid sections were imaged with either a Leica DMi8 fluorescence microscope or a Leica Sp8 confocal microscope at the Case Western Reserve School of Medicine Imaging Core. For counting of MYRF-positive nuclei, four 20× fields were imaged per spheroid. Two fields from the top and bottom of the spheroid and two fields from the edges of the central region of the spheroids were quantified (see Supplementary Fig. 1c for a schematic). The total numbers of DAPI-positive cells and MYRF-positive cells were manually counted in Adobe Photoshop or NIH ImageJ. Three to five spheroids were analyzed per line and treatment condition, and GraphPad Prism was used to perform a *t*-test to assess statistically significant differences between lines or treatments.

Electron microscopy. Spheroids were fixed and processed as previously described[52]. Samples were fixed for 1 h at room temperature in a fixative solution containing 4% paraformaldehyde (EMS), 2% glutaraldehyde (EMS), and 0.1 M Na-cacodylate (EMS). Samples were then osmicated, stained with uranyl acetate, and embedded in EMbed 812 (EMS). Ultrathin sections (120 nm) from each spheroid sample were observed with an FEI Helios NanoLab 660 FIBSEM field emission scanning electron microscope using extreme high resolution and equipped with a concentric (insertable) higher-energy electron detector. All images were taken using 4 kV and 0.2 current landing voltage at high magnification (15,000–35,000×).

Serial block-face imaging and 3D reconstruction. Epoxy-embedded spheroids were trimmed, mounted on silicon wafers, and covered with conductive silver paint. Using a sputter coating (Cressington Scientific Instruments), we deposited an additional ~1-nm iridium layer, and then we loaded samples into a Helios Nanolab 660i dual-beam microscope (FEI Company) for imaging. After the ion column and beam coincidence had been set up at the eucentric height (tilt, 52°), for the electron beam, 2 kV and 40 pA current landing were used, then ion beam (Ga+)-assisted platinum was deposited as a protective layer for subsequent milling for cross-sections using low current (0.23 nA), while surplus block material was removed with a high ion beam current (30 kV, 6.5 nA). For final surface polishing/milling, we used a reduced ion current (30 kV, 2.8 nA). For imaging, the Auto Slice and View G3 software (FEI Company) was used with an electron beam current of 400 pA and horizontal field width of 11.84 µm to acquire an image stack of 154 sections (pixel size, 1.97; $z = 50$ nm) using a through-the-lens detector, with a resolution of 6,144 × 4,096, dwell time of 6 µs, and working distance of 4.04 mm. Raw images were aligned in the Fiji image processing package, and Imaris 9.1 software (Bitplane AG) was used for image visualization and 3D reconstruction of myelin bundles.

Bulk RNA sequencing and analysis. Four spheroids per line were collected in TriReagent (Zymo Research; R2050-1-200), and RNA was extracted per the manufacturer's instructions. RNA was further purified with a Qiagen RNeasy Plus mini kit (Qiagen; 73404). Illumina libraries were prepared and sequenced in 50-bp paired-end mode on a HiSeq 2500 instrument at the CWRU Genomics Core facility. Reads were aligned to the hg19 genome with TopHat v2.0.6 without a reference transcriptome[53]. The abundance of transcripts from the iGenomes hg19 RefSeq reference was measured with Cufflinks v2.0.2[54]. FPKM values (fragments per kilobase of transcript per million mapped reads) were quantile-normalized. Neuron-, astrocyte-, and oligodendrocyte-specific genes were defined by expression (FPKM > 1) in their respective cells and absence in the other two lineages[27]. Each list was reduced to the 100 genes most specific to that cell type by fold change that were also detected in at least one spheroid sample. Differences in expression among gene lists were assessed by Wilcoxon test in GraphPad Prism.

Single-cell RNA sequencing and analysis. Ten independently generated week 12 spheroids were pooled and dissociated as previously described[55]. Briefly, we dissociated spheroids by using the Worthington Papain dissociation system (Worthington Biochemical Corp.; LK003150) according to the manufacturer's instructions. Papain solution was oxygenated with 95% O_2 and 5% CO_2 before dissociation. Cell counts of single-cell suspensions were obtained on a Countess automated cell counter (Invitrogen), and cells were loaded for single-cell capture at a final concentration of 1,000 cells per microliter.

Single-cell capture, cDNA synthesis, cDNA preamplification, and library preparation were carried out with the 10x Genomics Chromium Single Cell 3′ Library and Bead Kit v2 (10x Genomics; 120237). 3,850 cells were recovered and sequenced at a depth of 38,611 reads per cell with 1,870 median genes per cell. Cell Ranger Single-Cell Software Suite v2.1.0 was used for barcode processing and single-cell 3′ gene counting, and reads were mapped to hg19. Principal component analysis dimensionality reduction and *t*-distributed stochastic neighbor embedding analysis were performed by Cell Ranger Single-Cell Software Suite v2.1.0, and data were visualized with 10x Genomics Loupe Cell Browser v2.0.0. Data in Fig. 2 were clustered with 10x Genomics Loupe Cell Browser v2.0.0 using *k*-means clustering with a present number of two clusters to isolate broad clusters of neuronal and glial/progenitor cells. Clustering of spheroids was compared with publically available single-cell data from developing human cortex on UCSC Cluster Browser (http://bit.ly/cortexSingleCell)[36]. Oligocortical spheroid gene expression cluster heat maps in Fig. 2 were generated by 10x Genomics Loupe Cell Browser v2.0.0 and represent the $\log_2$ fold change of gene expression in each cell compared with the mean expression of that gene in the population as a whole. Comparative gene expression cluster heat maps of developing human cortex were generated from the UCSC Cluster Browser.

Statistics. To quantify the percentage of MYRF-positive oligodendrocytes in a single spheroid, we imaged four regions (as shown in Supplementary Fig. 2) and took the average percentage of MYRF-positive cells per spheroid. For data shown in Fig. 1, five spheroids ($n=5$) were analyzed similarly per treatment group. For data shown in Fig. 4, four spheroids were analyzed in each group ($n=4$). Data presented in Fig. 5m were obtained from five ($n=5$) spheroids of line CWRU198 and four spheroids from each PMD line ($n=4$). A two-tailed unpaired *t*-test with Welch's correction was performed to compare two groups at a time.

Bulk RNA-seq was performed with five spheroids from each condition. Paired nonparametric Wilcoxon matched-pairs signed-rank test was used to determine statistical significance.

Reporting Summary. Further information on experimental design is available in the Nature Research Reporting Summary linked to this article.

Data availability. All RNA-seq data have been deposited to the Gene Expression Omnibus (GEO) database under accession number GSE110006. The datasets generated and analyzed during the current study are available from the corresponding author on reasonable request.

References

51. Sheng, Y. et al. Using iPSC-derived human DA neurons from opioid-dependent subjects to study dopamine dynamics. *Brain Behav.* **6**, e00491 (2016).
52. Najm, F. J. et al. Rapid and robust generation of functional oligodendrocyte progenitor cells from epiblast stem cells. *Nat. Methods* **8**, 957–962 (2011).
53. Trapnell, C., Pachter, L. & Salzberg, S. L. TopHat: discovering splice junctions with RNA-Seq. *Bioinformatics* **25**, 1105–1111 (2009).
54. Trapnell, C. et al. Transcript assembly and quantification by RNA-seq reveals unannotated transcripts and isoform switching during cell differentiation. *Nat. Biotechnol.* **28**, 511–515 (2010).
55. Marques, S. et al. Oligodendrocyte heterogeneity in the mouse juvenile and adult central nervous system. *Science* **352**, 1326–1329 (2016).

nature research

Corresponding author(s): Paul Tesar

Life Sciences Reporting Summary

Nature Research wishes to improve the reproducibility of the work that we publish. This form is intended for publication with all accepted life science papers and provides structure for consistency and transparency in reporting. Every life science submission will use this form; some list items might not apply to an individual manuscript, but all fields must be completed for clarity.

For further information on the points included in this form, see Reporting Life Sciences Research. For further information on Nature Research policies, including our data availability policy, see Authors & Referees and the Editorial Policy Checklist.

Please do not complete any field with "not applicable" or n/a. Refer to the help text for what text to use if an item is not relevant to your study.
For final submission: please carefully check your responses for accuracy; you will not be able to make changes later.

Experimental design

1. Sample size

Describe how sample size was determined.

No statistical test was used to predetermine sample size. n= 4 or 5 spheroids were used per group per treatment in order to be able to perform statistical tests.

2. Data exclusions

Describe any data exclusions.

No data was excluded from any experiments presented in the paper

3. Replication

Describe the measures taken to verify the reproducibility of the experimental findings.

Spheroids were grown from 2 hES cell lines as well as 2 hiPS cell lines to establish this protocol and these results were reproduced with two additional batches from each of these lines. Additionally, this method was independently replicated in the Fossati lab.

4. Randomization

Describe how samples/organisms/participants were allocated into experimental groups.

Spheroids were generated in bulk until day 50 at which time they were randomly assigned to treatment groups.

5. Blinding

Describe whether the investigators were blinded to group allocation during data collection and/or analysis.

Spheroid treatment experiments were not blinded since initial variations in treatment were performed to optimize a method and not to test a hypothesis. To verify the robustness of the method, downstream analysis such as EM were blinded. Samples for EM were blinded to experimenters performing imaging and analysis.

Note: all in vivo studies must report how sample size was determined and whether blinding and randomization were used.

6. Statistical parameters

For all figures and tables that use statistical methods, confirm that the following items are present in relevant figure legends (or in the Methods section if additional space is needed).

n/a	Confirmed
☐	☒ The exact sample size (*n*) for each experimental group/condition, given as a discrete number and unit of measurement (animals, litters, cultures, etc.)
☐	☒ A description of how samples were collected, noting whether measurements were taken from distinct samples or whether the same sample was measured repeatedly
☐	☒ A statement indicating how many times each experiment was replicated
☐	☒ The statistical test(s) used and whether they are one- or two-sided *Only common tests should be described solely by name; describe more complex techniques in the Methods section.*
☐	☒ A description of any assumptions or corrections, such as an adjustment for multiple comparisons
☐	☒ Test values indicating whether an effect is present *Provide confidence intervals or give results of significance tests (e.g. P values) as exact values whenever appropriate and with effect sizes noted.*
☐	☒ A clear description of statistics including central tendency (e.g. median, mean) and variation (e.g. standard deviation, interquartile range)
☐	☒ Clearly defined error bars in all relevant figure captions (with explicit mention of central tendency and variation)

See the web collection on statistics for biologists for further resources and guidance.

Software

Policy information about availability of computer code

7. Software

Describe the software used to analyze the data in this study.	Microsoft excel and Graphpad Prism were used to graph and perform statistics. LASX was used for microscopy and Imaris 9.1 was used for EM visualization and 3D reconstruction.Adobe photoshop and NIH ImageJ were used for area calculations and counting. Cell Ranger and Loupe Browser software from 10X Genomics was used to analyze single cell data. TopHat v2.0.6 and Cufflinks v2.0.2 were used for analysis of bulk RNA -Seq data. Adobe Photoshop and Illustrator were used to assemble images.

For manuscripts utilizing custom algorithms or software that are central to the paper but not yet described in the published literature, software must be made available to editors and reviewers upon request. We strongly encourage code deposition in a community repository (e.g. GitHub). *Nature Methods* guidance for providing algorithms and software for publication provides further information on this topic.

Materials and reagents

Policy information about availability of materials

8. Materials availability

Indicate whether there are restrictions on availability of unique materials or if these materials are only available for distribution by a third party.	Human ES cell lines are available from their respective vendors. In house iPS cell lines are available upon request via a MTA with Case Western Reserve University.

9. Antibodies

Describe the antibodies used and how they were validated for use in the system under study (i.e. assay and species).	Primary antibodies used: rat-anti-PLP1 (1:500, AA3, gift from Wendy Macklin); rabbit-anti-MYRF (1:1000, gift from Dr. Michael Wegner); goat anti-SOX10 (1:250 R&D Systems AF 2864); rabbit anti-OLIG2 (1:250, Millipore AB9610; mouse-anti-pan-axonal neurofilament (1:1000, Covance #SMI311); mouse-anti-MBP (1:200, Covance # Smi99), mouse-anti-pan-neuronal neurofilament (NF, 1:1000, Covance #SMI312); rabbit-anti-GFAP (1:1000, Dako #Z0334); mouse anti-SATB2 (1:250, AbCam, #ab51520); rat anti-CTIP2 (1:400, AbCam #ab18465); goat anti-SOX2 (1:250 R&D Systems, #AF2018); rabbit anti-TBR2 (1:250, Abcam, ab23345); mouse anti-Ki67 (1:250, Millipore MAB4190); mouse anti-Nestin (1:250 Millipore, MAB5326); mouse anti-BrdU (1:1000, Millipore, MAB3510) chicken anti-Vimentin (1:1000 Abcam, ab24525). Antibody validation was based on previously published data or based on manufacturers recommendations. All secondary antibodies used were Alexa-Fluor conjugated secondary antibodies from Life Technologies and diluted 1:500. Secondary antibodies used : donkey anti rat Alexa Fluor 488(A-21208), donkey anti-mouse Alexa Fluor 488(A21202) , donkey anti-mouse Alexa Fluor 555 (A31570), donkey anti-mouse Alexa Fluor 647(A31571), donkey anti-rabbit Alexa Fluor 555(A31572), donkey anti-rabbit Alexa Fluor 647(A31573), goat anti -chicken 647(A21449), donkey anti-goat Alexa Fluor 488(A21432), donkey anti-goat 647(A21447).

10. Eukaryotic cell lines

a. State the source of each eukaryotic cell line used.	Embryonic stem cell lines H7 and H9 were sourced from WiCell and RUES1 was obtained from the Rockefeller University. CWRU191 and CWRU198 and PMD patient lines are in house iPSC lines generated at Case Western Reserve University.
b. Describe the method of cell line authentication used.	DNA Fingerprinting via Cell Line Genetics (Madison, WI)
c. Report whether the cell lines were tested for mycoplasma contamination.	Cell lines are checked monthly for mycoplasma contamination and no contamination was present.
d. If any of the cell lines used are listed in the database of commonly misidentified cell lines maintained by ICLAC, provide a scientific rationale for their use.	No commonly misidentified cell lines were used in this study

Animals and human research participants

Policy information about studies involving animals; when reporting animal research, follow the ARRIVE guidelines

11. Description of research animals

Provide all relevant details on animals and/or animal-derived materials used in the study.	No animals were used in this study.

Policy information about studies involving human research participants

12. Description of human research participants

Describe the covariate-relevant population characteristics of the human research participants.	There are no human research participants in this study.